Collisional Activation of Pyrene and Anthracene in an Ion-Trap Mass Spectrometer

B. D. Nourse, K. A. Cox, K. L. Morand, and R. G. Cooks*

Contribution from the Chemistry Department, Purdue University, West Lafayette, Indiana 47907.
Received May 1, 1991

Abstract: A quadrupole ion-trap mass spectrometer (ITMS) has been used to examine internal energy deposition and fragmentation pathways of ionized pyrene and anthracene. Through multiple collisional activation steps, large amounts of energy (tens of electronvolts) can be deposited and multiple-stage (MS^n) dissociation reactions such as $C_{16}H_{10}^{\bullet+} \rightarrow C_{16}H_9^+ \rightarrow C_{16}H_8^{\bullet+} \rightarrow C_{14}H_6^{\bullet+} \rightarrow C_{12}H_4^{\bullet+} \rightarrow C_8H_2^{\bullet+} \rightarrow C_3H_2^{\bullet+}$ are observed. This particular reaction sequence requires approximately 29 eV, as estimated from the energy requirements for the individual dissociation reactions. While each individual reaction has an activation energy <8 eV, the occurrence of the reaction sequence demonstrates the large total amount of energy which can be delivered in these experiments. The intriguing chemistry made accessible by multiple-stage activation (up to MS^{10}) is exemplified by the formation of all-carbon fragment ions such as $C_7^{\bullet+}$ from the polycyclic aromatic hydrocarbon molecular ions. Under extreme activation conditions (high amplitude of the excitation pulse and longer activation time), the fragment ions observed in a single-stage (MS/MS) experiment include those having estimated activation energies as high as 17 eV. High-energy pathways can also be directly accessed in single-stage MS/MS experiments under less extreme activation conditions by introducing a small amount of xenon as the target gas with the helium buffer. This method has the additional advantage of high dissociation efficiency.

Introduction

Polycyclic aromatic hydrocarbons (PAHs) are one of the largest classes of environmental carcinogens.[1,2] They are formed by combustion, principally of fossil or synthetic fuels, making them widespread contaminants.[3] The planar structure of these compounds makes it possible for them to intercalate between DNA base pairs, inhibiting replication.[4] In at least some cases, their mutagenic effects have been linked to the production of diol-epoxide derivatives which bind covalently with DNA bases.[3,5] PAH radical cations also bind covalently to DNA through one-electron oxidation.[6] In view of this and the role of mass spectrometry in the analysis of these compounds,[2,7] there continues to be a strong interest in the ion chemistry of PAHs.

Because of the unusual structural stability of PAHs, a substantial amount of internal energy is required to cause extensive fragmentation.[7-9] This is evident from mass spectra recorded using ionization methods such as electron ionization (EI)[8,10] and multiphoton resonance ionization (MPRI),[11] and from tandem mass spectrometry (MS/MS) experiments performed using a variety of activation techniques,[7] such as collision-activated dissociation (CAD) at high (keV) and low (eV) ion kinetic energies with gaseous targets[12] and collisions with surfaces (SID),[7,13-18] as well as photodissociation (PD)[13] and electron-impact excitation.[19] In low-energy collisional-activation studies,[12,20] minimal fragmentation is observed,[10,21,22] although losses of one or more hydrogen atoms are observed. These processes typically give the most abundant fragments in all activation experiments, while losses of C_2H_n neutrals (particularly C_2H_2 and C_2H_4) are also commonly observed. Although high-energy (keV range) collisions might be expected to deposit much larger internal energies into mass-selected organic ions, they typically deposit an average of approximately 3 eV of internal energy into the ion, while the high-energy tail of the internal energy distribution can extend beyond 15 eV.[23-26] As a result of this tail, several fragment ions which arise by high-energy processes are observed in high-energy, but not low-energy, CAD spectra. They include $C_nH_2^{\bullet+}$ and $C_nH_3^+$ ions, prominent at lower mass, and $C_nH_6^{\bullet+}$ and $C_nH_7^+$ fragment ions, which tend to be more prominent in the higher mass region.[7] These fragments, which are characteristic of all PAHs, suggest that fragmentation proceeds by isomerization to yield common intermediate structures.[7]

Differentiation of isomeric PAHs is a problem of practical importance, but CAD is seldom successful,[27-35] although charge

(1) *Handbook of Polycyclic Aromatic Hydrocarbons*; Bjørseth, A., Ed.; Marcel Dekker, Inc.: New York, 1983; Vol. 1.
(2) Lee, M. L.; Novotny, M. V.; Bartle, K. D. *Analytical Chemistry of Polyaromatic Hydrocarbons*; Academic Press: New York, 1981.
(3) *Polynuclear Aromatic Hydrocarbons*; *Vol. 1 of Carcinogenesis—A Comprehensive Survey*; Freudenthal, R. I., Jones, P. W., Eds.; Raven Press: New York, 1976; p 1.
(4) Waring, M. J. *Annu. Rev. Biochem.* **1981**, *50*, 159.
(5) Jerina, D. M.; Daly, J. W. *Science* **1974**, *185*, 537.
(6) Rogan, E. G.; Cavalieri, E. L.; Tibbels, S. R.; Cremonesi, P.; Warner, C. D.; Nagel, D. L.; Tomer, K. B.; Cerny, R. L.; Gross, M. L. *J. Am. Chem. Soc.* **1988**, *110*, 4023.
(7) Pachuta, S. J.; Kenttämaa, H. I.; Sack, T. M.; Cerny, R. L.; Tomer, K. B.; Gross, M. L.; Pachuta, R. R.; Cooks, R. G. *J. Am. Chem. Soc.* **1988**, *110*, 657.
(8) Natalis, P.; Franklin, J. L. *J. Phys. Chem.* **1965**, *69*, 2935.
(9) Shushan, B.; Boyd, R. K. *Org. Mass Spectrom.* **1980**, *15*, 445.
(10) Wacks, M. E. *J. Chem. Phys.* **1964**, *41*, 1661.
(11) Hrubowchak, D. M.; Ervin, M. H.; Winograd, N. *Anal. Chem.* **1991**, *63*, 225.
(12) *Tandem Mass Spectrometry*; McLafferty, F. W., Ed.; John Wiley and Sons: New York, 1983.
(13) Mabud, M. A.; DeKrey, M. J.; Cooks, R. G. *Int. J. Mass Spectrom. Ion Processes* **1985**, *67*, 285.
(14) Bier, M. E.; Schwartz, J. C.; Schey, K. L.; Cooks, R. G. *Int. J. Mass Spectrom. Ion Processes* **1990**, *103*, 1.
(15) Cooks, R. G.; Ast, T.; Mabud, M. A. *Int. J. Mass Spectrom. Ion Processes* **1990**, *90*, 3120.
(16) Schey, K. L.; Cooks, R. G.; Kraft, A.; Grix, R.; Wollnik, H. *Int. J. Mass Spectrom. Ion Processes* **1989**, *94*, 1.
(17) Ast, T.; Mabud, M. A.; Cooks, R. G. *Int. J. Mass Spectrom. Ion Processes* **1988**, *82*, 131.
(18) Bier, M. E.; Amy, J. W.; Cooks, R. G.; Syka, J. E. P.; Ceja, P.; Stafford, G. C. *Int. J. Mass Spectrom. Ion Processes* **1987**, *77*, 31.
(19) Cody, R. B.; Freiser, B. S. *Anal. Chem.* **1979**, *51*, 547.
(20) *Mass Spectrometry/Mass Spectrometry: Techniques and Applications of Tandem Mass Spectrometry*; Busch, K. L., Glish, G. L., McLuckey, S. A., Eds.; VCH Publishers, Inc.: New York, 1988.
(21) Wacks, M. E.; Dibeler, V. H. *J. Chem. Phys.* **1959**, *31*, 1557.
(22) Hase, A.; Lin, P. H.; Hites, R. A. In *Polynuclear Aromatic Hydrocarbons*; *Vol. 1 of Carcinogenesis—A Comprehensive Survey*; Freudenthal, R. I., Jones, P. W., Eds.; Raven Press: New York, 1976; p 435.
(23) Wysocki, V. H.; Kenttämaa, H. I.; Cooks, R. G. *Int. J. Mass Spectrom. Ion Processes* **1987**, *75*, 181.
(24) Kenttämaa, H. I.; Cooks, R. G. *Int. J. Mass Spectrom. Ion Processes* **1985**, *64*, 79.
(25) Kim, B. J.; Kim, M. S. *Int. J. Mass Spectrom. Ion Processes* **1990**, *98*, 193.
(26) Kim, M. S.; McLafferty, F. L. *J. Am. Chem. Soc.* **1978**, *100*, 3279.
(27) Sim, P. G.; Jamieson, W. D.; Boyd, R. K. *Org. Mass Spectrom.* **1989**, *24*, 327.
(28) Dass, C.; Sack, T. M.; Gross, M. L. *J. Am. Chem. Soc.* **1984**, *106*, 5780.
(29) Keough, T. *Anal. Chem.* **1982**, *54*, 2540.
(30) Stemmler, E. A.; Buchanan, M. V. *Rapid Commun. Mass Spectrom.* **1988**, *2*, 184.
(31) Stemmler, E. A.; Buchanan, M. V. *Org. Mass Spectrom.* **1989**, *24*, 94, 705.
(32) Zakett, D.; Ciupek, J. D.; Cooks, R. G. *Anal. Chem.* **1981**, *53*, 723.
(33) Buchanan, M. V.; Rubin, I. B.; Wise, M. B.; Glish, G. L. *Biomed. Environ. Mass Spectrom.* **1987**, *14*, 395.
(34) Buchanan, M. V.; Olerich, G. *Org. Mass Spectrom.* **1984**, *19*, 486.

0002-7863/92/1514-2010$03.00/0

stripping[36,37] is sometimes useful, and certain ion/molecule reactions permit structural distinction.[29] Dimethyl ether molecular ions, for example, react with some PAHs to form $(M + C_2H_5O)^+$ adducts to an extent which depends strongly on the degree of loss of resonance energy accompanying the cycloaddition reaction.[29] Furthermore, surface-catalyzed oxidation reactions can be used to differentiate certain PAHs and their methyl derivatives under negative-ionization conditions.[31] Electron capture negative chemical ionization has also been used to differentiate isomeric PAHs through differences in electron affinity.[34] In addition, Hückel molecular orbital theory has been used recently to calculate relative carbon–hydrogen bond dissociation energies for PAHs.[38] The results allow estimations of proton affinities to be made which are dependent on the chemical structure and the site of protonation.[38]

The present work arose from a desire to utilize the unique capabilities of the quadrupole ion-trap mass spectrometer (ITMS) to contribute to the understanding of the mass spectrometry of PAHs through energy deposition studies and through the delineation of fragmentation pathways. The PAHs also serve as a convenient system to define some of the characteristics of the ion trap, especially in regard to energy transfer, a key consideration in structure elucidation by mass spectrometry. The ITMS is a device[39] in which ions can be mass selected and collided with a gas to cause dissociation or reaction and the products mass analyzed.[40–42] This tandem mass spectrometry (MS/MS) experiment can be repeated several times to allow a sequence of reactions to be studied in an MS^n experiment.[43–45]

From previous work,[39] it is known that the amount of internal energy deposited in a selected ion in the ion trap can be varied by altering the activation time or the amplitude of the activating voltage. Hence, even though low-energy collisions occur,[39,46] internal energies deposited are estimated to range up to 6 eV for the tetraethylsilane radical cation,[39] while processes which require 5.8 eV are observed for dimethyl phosphite molecular ions. These processes occur as a result of multiple energetic collisions with the helium buffer gas, the effects of which are additive and raise the internal energy of the activated ion.[46] Recent studies indicate that higher energy dissociation pathways can be accessed by the use of alternative target gases such as argon,[47] or by using a mixture of target gases (helium/argon or helium/xenon).[48–50] Collisions with a heavy target gas result in increased internal energy deposition in the activated ion; however, this occurs at the expense of trapping efficiency,[47–49] and such methods appear not to have been widely adopted.

MS^n experiments provide another means of accessing higher energy dissociation pathways. One purpose of this study is to assess the degree to which the MS^n capabilities of the ion trap allow the internal energy deposition to be increased. Not only is this of interest in mapping out the fragmentations of PAHs, but high-energy deposition is perceived increasingly as important[51] in obtaining structural information on biological compounds by mass spectrometry.

Scheme I

m/z 202 —> m/z 201 —> m/z 200 —> m/z 174 —> m/z 148 —> m/z 98 —> m/z 62

$$C_{16}H_{10}^{+\cdot} \xrightarrow{-H^{\cdot}} C_{16}H_9^{+} \xrightarrow{-H^{\cdot}} C_{16}H_8^{+\cdot} \xrightarrow{-C_2H_2} C_{14}H_6^{+\cdot} \xrightarrow{-C_2H_2} C_{12}H_4^{+\cdot} \xrightarrow{-C_4H_2} C_8H_2^{+\cdot} \xrightarrow{-C_3} C_5H_2^{+\cdot}$$

ϵ_0 (eV) = 7.2±0.7 (0.6±?.3) 6.0±1.0 3.9±0.9 2.7±0.4 6.5±0.4

Experimental Section

Experiments were performed using a prototype Finnigan ion-trap mass spectrometer (ITMS).[39–41] Electron ionization was employed (typically for 10 ms), and the application of rf and dc voltages to the ring and endcap electrodes of the ITMS allowed single ion isolation, collision activated dissociation, and mass selective instability experiments to be performed. Parent ions were isolated by setting the rf voltage such that the value of the Mathieu parameter, q_z, was 0.781 and then applying a dc voltage to the ring electrode (typically −215 volts for 7 ms in the case of $C_{16}H_{10}^{+\cdot}$; this dc voltage is mass dependent). The q_z value was then reduced and mass-selected ions were dissociated using collisional activation by applying a supplementary ac voltage across the endcap electrodes at the fundamental frequency of the chosen ions, leading to dissociation upon collision with the helium buffer gas. An ac voltage of approximately 1 V_{p-p} was applied to each isolated ion for 50 ms at a value of q_z equal to 0.26 and at a frequency which varied with the m/z value, and ranged between 70 and 170 kHz. The exact frequency varied slightly with experimental conditions and was adjusted to optimize each dissociation step. The resulting products were then mass-analyzed by a mass selective instability scan induced by an rf voltage ramp (0–15 kV_{p-p}). Conditions for the extremely high energy CAD experiments were 12 V_{p-p} ac voltage applied for 100 ms. CAD experiments comparing the effects of mixed target gases (nominal pressure $1-5 \times 10^{-5}$ Torr of xenon and 1.5×10^{-4} Torr of helium) with those involving helium alone (1.5×10^{-4} Torr) utilized a forward rf scan for isolation of the parent ion from lower mass ions rather than the rf/dc method described above. Isolation of the parent ion from higher mass ions was not performed in this case. Resonance ejection[52] was employed in these comparable studies (530 kHz, 12 V_{p-p}) during spectral acquisition, for enhanced mass resolution.

Solid samples were introduced into the ion trap via a direct-insertion probe which was heated between 80 and 105 °C. The helium damping gas was introduced using a Granville–Phillips valve, yielding a total operating pressure of $1.5-2 \times 10^{-4}$ Torr (uncorrected), as measured in the vacuum manifold using a Bayard–Alpert ionization gauge. Xenon was also introduced through a Granville–Phillips valve at a pressure of $1-5 \times 10^{-5}$ Torr (uncorrected) and was present throughout the entire scan sequence in these experiments. The samples were obtained commercially and were not specially purified.

Results

Shown in Figure 1 are some of the dissociation pathways for ionized pyrene as determined using collision-activated dissociation in an ITMS. Note that molecular formulas are assigned on the basis of nominal mass; they are not directly measured but are consistent with data taken on d_{10}-pyrene, the spectra of which display the expected mass shifts. Neutral fragments commonly lost from the selected parent ions are $H^{\cdot}$, H_2, C_2H_2, C_2H_4, and C_4H_2, and less common fragments, also seen, are C_6H_2, C_8H_2, and C_3. The longest sequence of dissociations observed to originate from one ionization event is represented by nine separate isolation and activation steps (viz., an MS^{10} experiment). Using multiple activation steps, m/z 202 ($C_{16}H_{10}^{+\cdot}$) was dissociated by sequential loss of $H^{\cdot}$, $H^{\cdot}$, C_4H_2, $H^{\cdot}$, C_2H_2, $H^{\cdot}$, $H^{\cdot}$, $H^{\cdot}$, and C_3 to yield m/z 84 ($C_7^{+\cdot}$). Note that some ions have multiple origins and m/z 98, for example, is formed by at least three different dissociation pathways.

Figure 2 shows the CAD product ion spectra recorded for an MS^6 dissociation sequence which converts $C_{16}H_{10}^{+\cdot}$ to $C_5H_2^{+\cdot}$. The selected parent ions are shown in parentheses at the right of

(35) Shushan, B.; Safe, S. H.; Boyd, R. K. *Anal. Chem.* **1979**, *51*, 156.
(36) Dass, C.; Peake, D. A.; Gross, M. L. *Org. Mass Spectrom.* **1986**, *21*, 741.
(37) Holmes, J. L.; Terlouw, J. K.; Burgers, P. C. *Org. Mass Spectrom.* **1980**, *15*, 149.
(38) Stein, S. E.; Brown, R. L. *J. Am. Chem. Soc.* **1991**, *113*, 787.
(39) Louris, J. N.; Cooks, R. G.; Syka, J. E. P.; Kelley, P. E.; Stafford, G. C.; Todd, J. F. J. *Anal. Chem.* **1987**, *59*, 1677.
(40) Nourse, B. D.; Cooks, R. G. *Anal. Chim. Acta* **1990**, *228*, 1.
(41) Todd, J. F. J. *Mass Spectrom. Rev.* **1991**, *10*, 3.
(42) March, R. E.; Hughes, R. J. *Quadrupole Storage Mass Spectrometry*; John Wiley and Sons: New York, 1989.
(43) Louris, J. N.; Brodbelt, J. S.; Cooks, R. G.; Glish, G. L.; VanBerkel, G. J.; McLuckey, S. A. *Int. J. Mass Spectrom. Ion Processes* **1990**, *96*, 117.
(44) Glish, G. L.; McLuckey, S. A.; Asano, K. G. *J. Am. Soc. Mass Spectrom.* **1990**, *1*, 166.
(45) McLuckey, S. A.; Glish, G. L.; VanBerkel, G. J. *Int. J. Mass Spectrom. Ion Processes* **1991**, *106*, 213.
(46) Brodbelt, J. S.; Kenttämaa, H. I.; Cooks, R. G. *Org. Mass Spectrom.* **1988**, *23*, 6.
(47) Gronowska, J.; Paradisi, C.; Traldi, P.; Vettori, U. *Rapid Commun. Mass Spectrom.* **1990**, *4*, 306.
(48) Glish, G. L.; McLuckey, S. A.; Goeringer, D. E.; Van Berkel, G. J.; Hart, K. J. Proceedings of the 39th ASMS Conference on Mass Spectrometry and Allied Topics, Nashville, TN, 1991; p 536.
(49) McLuckey, S. A.; Glish, G. L.; Asano, K. G. *Anal. Chim. Acta* **1989**, *225*, 25.
(50) Morand, K. L.; Hoke, S. H.; Eberlin, M. N.; Payne, G.; Cooks, R. G. *Org. Mass Spectrom.*, in press.
(51) *Mass Spectrometry of Peptides*; Desiderio, D. M., Ed.; CRC Press, Inc.: Boston, MA, 1991.
(52) Kaiser, R. E.; Louris, J. N.; Amy, J. W.; Cooks, R. G. *Rapid Commun. Mass Spectrom.* **1989**, *3*, 225.

Table I. Ion Yields, Efficiencies, and Relative Abundances in the Sequential Dissociation of Pyrene

parent ions	fragment[a] ions (m/z)	selected[b] ion (m/z)	yield[c] %	% relative[d] abundance	CAD[e] efficiency
202	201, 200, 176	200	49	49	53
200	199, 198, 175, 174	174	11[f]	5.4[f]	71
174	173, 148	148	38	2.0	79
148	122, 98	98	35	0.13	54
98	97, 62	62	13	0.065	37

[a] Fragment ions formed upon CAD of the selected parent ion in the first column. [b] The fragment ion selected for the next dissociation step. [c] The yield of the selected ion (column three) from the preceding step (determined from relative abundances). [d] The relative abundance of the fragment ion (column three) with respect to the abundance of m/z 202. [e] A ratio of the sum of the fragment ion intensities to the parent ion intensity for each dissociation step. [f] When a dc voltage is applied in order to isolate m/z 174, space charge problems are eliminated and the peak "sharpens up"; hence, the peak height increases significantly (% yield and % relative abundance before dc isolation were 7% and 3.6%, respectively). All calculations are estimated by peak height measurements, and peaks have 1-Da resolution unless otherwise stated.

Table II. Fragment Ions, Relative Abundances, and CAD Efficiencies of Single-Step MS/MS Experiments Using Rf/Dc Isolation[a]

experimental CAD conditions	fragment ion (relative abundance)	total CAD efficiency (%)
1.5×10^{-4} Torr of He, 12 V_{p-p}, 50 ms	202 (5), 198 (100), 197 (56), 193 (2), 187 (5), 176 (4), 175 (5), 174 (39), 173 (4), 172 (3), 169 (2), 152 (2), 151 (2), 150 (20), 149 (2), 148 (2)	21
1.5×10^{-4} Torr of He, 12 V_{p-p}, 100 ms	202 (8), 198 (37), 197 (100), 196 (7), 193 (5), 187 (28), 185 (5), 176 (6), 175 (6), 174 (51), 173 (6), 172 (10), 171 (4), 169 (6), 167 (4), 152 (4), 151 (4), 150 (28), 149 (6), 148 (6)	34
1.5×10^{-4} Torr of He, 1.0×10^{-5} Torr of Xe, 12 V_{p-p}, 50 ms	196 (25), 174 (100), 173 (25), 172 (25), 171 (62), 150 (75), 149 (34), 148 (38), 147 (38), 146 (48), 123 (26), 122 (38)	31
1.5×10^{-4} Torr of He, 1.0×10^{-5} Torr of Xe, 12 V_{p-p}, 100 ms	199 (6), 198 (100), 197 (12), 189 (2), 176 (5), 175 (9), 174 (33), 173 (6), 172 (2), 169 (2), 167 (2), 163 (2), 152 (3), 151 (6), 150 (22), 149 (10), 148 (2), 147 (2), 146 (2), 126 (2), 123 (2), 122 (3), 101 (1), 98 (1)	20

[a] Parent ion: m/z 202.

Table III. Fragment Ions, Relative Abundances, and CAD Efficiencies of Single-Step MS/MS Experiments Using Rf-Only Isolation[a]

experimental CAD conditions	fragment ion (relative abundance)	total CAD efficiency (%)
1.5×10^{-4} Torr of He, 12 V_{p-p}, 50 ms	200 (6), 199 (100), 198 (43), 193 (1), 189 (1), 187 (1), 176 (3), 175 (5), 174 (18), 152 (2), 151 (3), 150 (6)	56
1.5×10^{-4} Torr of He, 12 V_{p-p}, 100 ms	200 (1), 199 (50), 198 (100), 193 (1), 189 (1), 188 (1), 187 (2), 177 (1), 176 (3), 175 (5), 174 (22), 169 (1), 152 (1), 151 (2), 150 (6), 149 (1)	52
1.5×10^{-4} Torr of He, 1.0×10^{-5} Torr of Xe, 12 V_{p-p}, 50 ms	199 (6), 198 (100), 197 (12), 189 (2), 176 (5), 175 (9), 174 (33), 173 (6), 172 (2), 169 (2), 167 (2), 163 (2), 152 (3), 151 (6), 150 (22), 149 (10), 148 (2), 147 (2), 146 (2), 126 (2), 123 (2), 122 (3), 101 (1), 98 (1)	54
1.5×10^{-4} Torr of He, 1.0×10^{-5} Torr of Xe, 12 V_{p-p}, 100 ms	198 (15), 197 (22), 196 (37), 193 (7), 191 (7), 187 (15), 185 (15), 176 (19), 175 (19), 174 (100), 173 (19), 172 (31), 171 (56), 170 (10), 169 (19), 167 (7), 165 (7), 164 (19), 163 (30), 159 (7), 158 (7), 152 (11), 151 (11), 150 (100), 149 (20), 148 (20), 147 (33), 146 (33), 139 (4), 137 (2), 135 (4), 134 (7), 133 (2), 126 (6), 125 (3), 124 (7), 123 (30), 122 (48), 121 (3), 120 (3), 111 (4), 110 (3), 109 (3), 101 (3), 99 (3), 98 (4), 97 (7)	57

[a] Parent ion: m/z 202.

each spectrum, and the ion abundance is shown in arbitrary units at the left. These data represent optimum conditions for each CAD product spectrum (i.e., optimized rf levels, activation amplitudes, and activation time); hence, this figure includes data from a number of separate experiments. For a single MS[6] experiment in which the sequence m/z 202 → m/z 200 → m/z 174 → m/z 148 → m/z 98 → m/z 62 occurs, the overall yield of the product ion (m/z 62) is 0.065% (Table I). Table I lists the CAD efficiencies for each consecutive dissociation step, the relative abundance of each selected ion with respect to the abundance of m/z 202, and the overall ion yields. CAD efficiencies are defined as the sum of the measured fragment ion abundances divided by the parent ion abundance measured prior to activation.[39,53] All values are estimated using peak heights at unit mass resolution. Note that not all the fragment ions illustrated in Figure 1 appear in the spectra of the selected parent ions shown in Table I. This is again because Table I represents the results of a single consecutive experiment in which experimental conditions remain constant, whereas experimental conditions (collision time and ac activation amplitude) were separately optimized for each successive fragment ion spectrum in Figure 1.

The energetics of one of the reaction pathways in Figure 1 is illustrated in Scheme I. The neutral losses are shown above the arrows while the critical energies, ϵ_o, for each dissociation step are shown below the arrows. The critical energies are approximated from the enthalpy change ($\Delta(\Delta H_f)$) for each dissociation reaction; estimates for the ionic heats of formation were often necessary (see supplementary material). Although each individual dissociation step in this particular sequence requires <8.0 eV, the total energy required to produce $C_5H_2^{\bullet+}$ (calculated from the sum of the ϵ_o values) is 29 ± 2 eV.

The CAD product spectrum of the pyrene radical cation ($C_{16}H_{10}^{\bullet+}$), taken under extreme activation conditions, is shown in Figure 3. In this experiment, a single 12-V_{p-p} excitation voltage pulse was applied at the resonance frequency of the $C_{16}H_{10}^{\bullet+}$ ion for 100 ms (versus 1 V_{p-p} for 50 ms for all other data shown here). Note the formation of m/z 122 ($C_{10}H_2^{\bullet+}$), a process which requires an energy estimated to be between 17.3 eV and 21.9 eV, depending on the pathway connecting parent and product (see supplementary material for these values and how they were estimated). The CAD efficiency under these unusually high energy dissociation conditions is 7%.

When an identical experiment was performed with the addition of 1×10^{-5} Torr of xenon to the helium buffer gas,[50] higher internal energies were deposited into the $C_{16}H_{10}^{\bullet+}$ ion under conditions *less* extreme than those described above. A supplementary ac voltage was applied at 12 V_{p-p} for only 50 ms. As a result, the higher energy fragmentation pathways were observed

(53) Yost, R. A.; Enke, C. G. *Anal. Chem.* **1979**, *51*, 1251A.

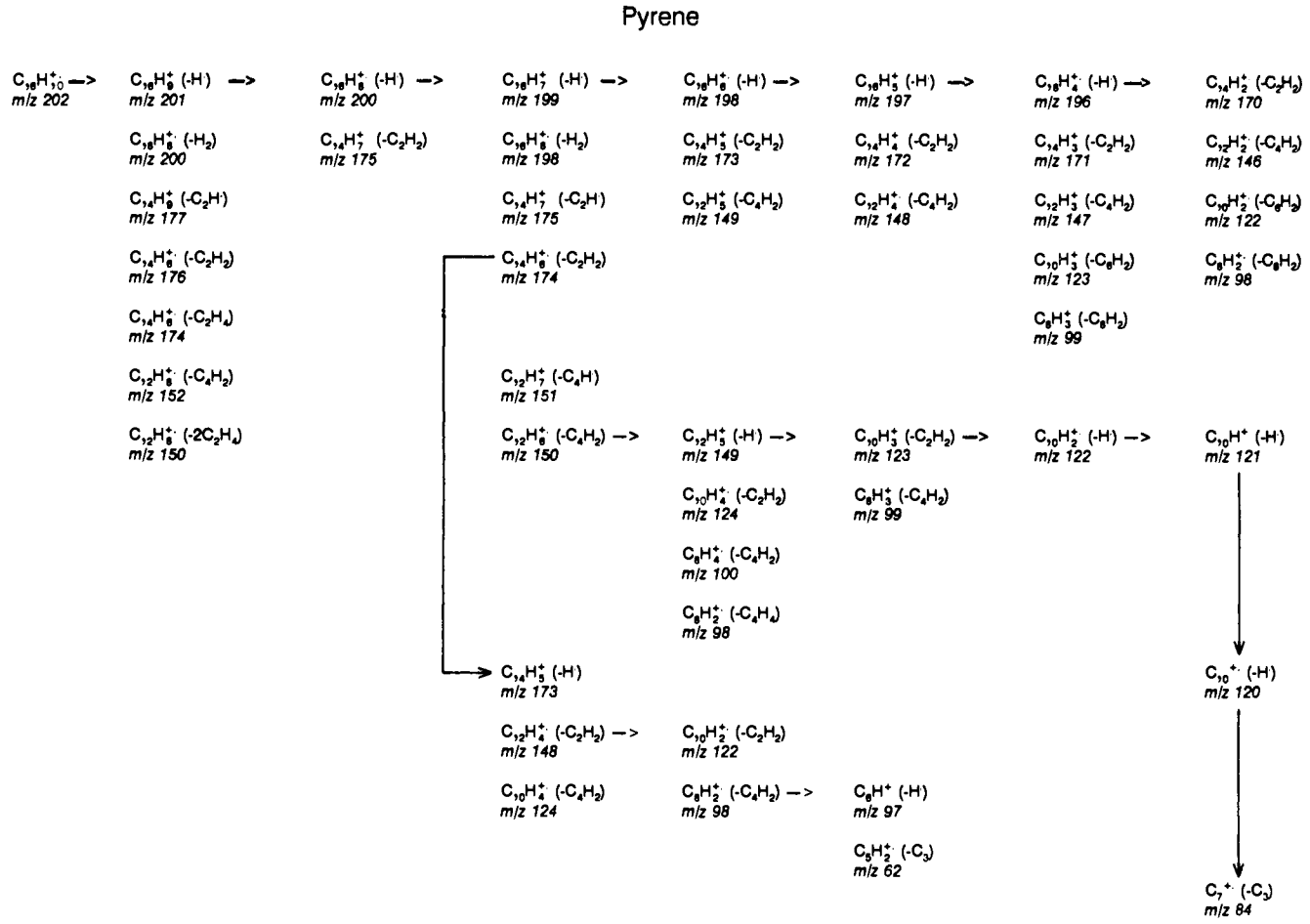

Figure 1. Consecutive dissociation pathways of ionized pyrene determined by using CAD in an ITMS. An ac amplitude of 1 V_{p-p} was applied to each isolated ion for 50 ms to effect activation.

Scheme II

$$C_{16}H_{10}^{\cdot +\,+} \xrightarrow{-C_2H_2} C_{14}H_8^{\cdot +\,+} \xrightarrow{-C_2H_2} C_{12}H_6^{\cdot +\,+} \xrightarrow{-C_2H_2} C_{10}H_4^{\cdot +\,+} \longrightarrow C_3H_3^{+} + C_7H^{+}$$

with a much higher dissociation efficiency. Tables II and III compare the effect of isolation by the standard rf/dc procedure vs rf-only isolation in 100- and 50-ms-activation MS/MS experiments. The reasons for the observed differences are discussed below.

The dissociation pathways for doubly-charged pyrene were also explored using the MS^n capabilities of the ITMS. One reaction sequence is shown in Scheme II. The pyrene dication fragments by loss of neutral C_2H_2 to give smaller dications, which ultimately undergo charge separation in the last CAD step, to yield two monocations.

Ionized anthracene behaves very similarly to pyrene as illustrated in Figure 4. Neutrals commonly lost are H·, C_2H_2, and C_4H_2; and the longest sequence of dissociations is represented by nine separate isolation and activation steps which convert $C_{14}H_{10}^{\cdot +}$ to $C_7^{\cdot +}$ in an overall yield of 0.34%. Listed in Table IV are the CAD efficiencies, relative abundances, and ion yields for the MS^{10} experiment on anthracene.

Discussion

The capabilities of the ITMS for multiple stages of ion isolation and activation are demonstrated by the results shown in Figure 1. The MS^n capabilities not only allow deposition (in stages) of sufficient internal energy to generate ions which require extremely high energies for formation but also provide information on the fragmentation sequences involved. The longest sequence of dissociation reactions is represented by nine separate isolation and activation events (MS^{10}), which convert the molecular ion, m/z 202, to the $C_7^{\cdot +}$ ion, m/z 84. While the degree of excitation achieved here is greater, the fragment ions formed, and the neutral molecules lost are similar to those seen in other experiments with PAHs including SID,[7,14-18] keV CAD,[7,12] photodissociation,[13] multiphoton ionization,[7] and MPRI.[11] This is the case in spite of the facts that some of these processes involve a single energetic activation event, while the ITMS employs multiple stages of activation, and that multiple collisions with helium occur during each stage of CAD. The hypothesis[7] that much of the fragmentation of PAHs proceeds along common pathways through "common" ions, i.e., ions with the same m/z value which are generated by different fragmentation pathways from one or more selected precursors, derives support from these observations. For example, the common ion at m/z 150 ($C_{12}H_6^{\cdot +}$) is seen in the

Table IV. Ion Yields, Efficiencies, and Relative Abundances in the Sequential Dissociation of Anthracene

parent ions	fragment[a] ions (m/z)	selected[b] ion (m/z)	yield[c] %	% relative[d] abundance	CAD[e] efficiency
178	177, 152	177	26	26.2	67
177	176, 151	176	99	26.2	100
176	175, 150	150	37	7.2	89
150	149, 124, 100, 98	149	65	2.7	81
149	123, 99, 75	123	92	2.7	100
123	122	122	95	2.2	95
122	121	121	66	1.4	66
121	120	120	65	0.90	65
120	84	84	34	0.34	34

[a] Fragments formed upon CAD of the selected parent ion in the first column. [b] The fragment ion selected for the next dissociation step. [c] The yield of the selected fragment ion (column three) from the preceding step (determined from relative abundances). [d] The relative abundance of the fragment ion (column three) with respect to the abundance of m/z 178. [e] A ratio of the sum of the fragment ion abundances to the parent ion abundance for each dissociation step.

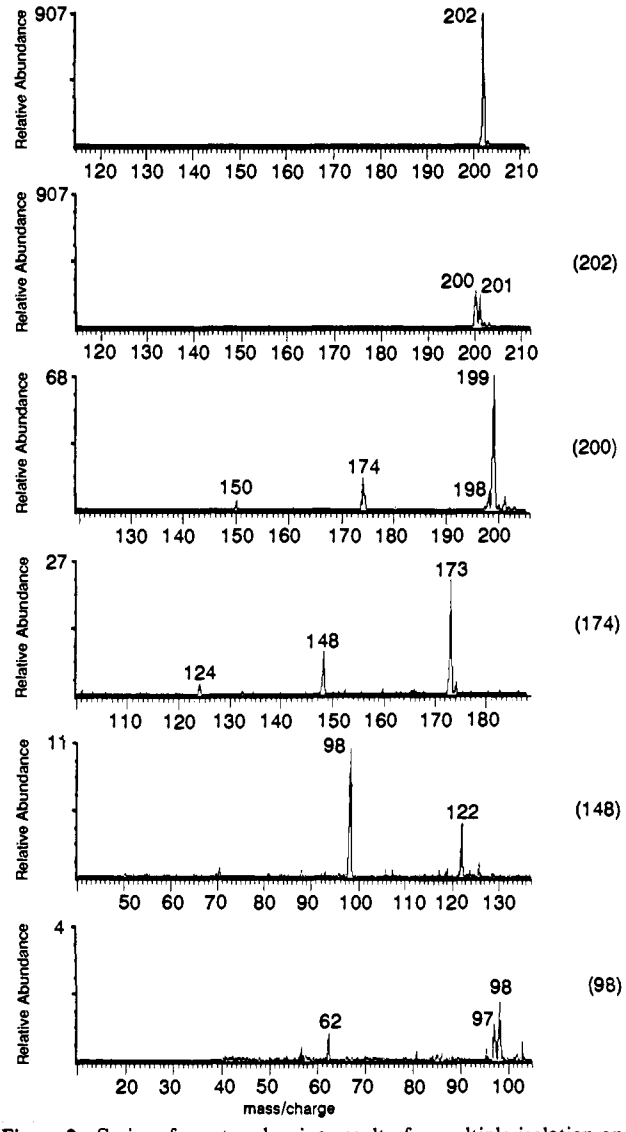

Figure 2. Series of spectra showing result of a multiple isolation and activation experiment (MS^6) for ionized pyrene. The molecular radical cation of pyrene ($C_{16}H_{10}^{\bullet+}$) is dissociated by a series of five separate steps (MS^6) to give an ion at m/z 62 ($C_5H_2^{\bullet+}$).

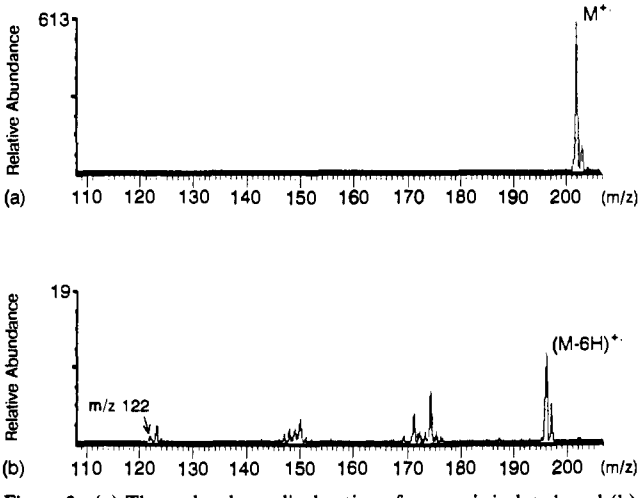

Figure 3. (a) The molecular radical cation of pyrene is isolated, and (b) under high energy activation conditions the resultant product ion spectrum is shown. An ac amplitude of 12 V_{p-p} was applied to $M^{\bullet+}$ for 100 ms.

mass and CAD spectra[7] of many PAHs as well as in the MS^n data for pyrene shown here. Similarly, the ion at m/z 98 ($C_8H_2^{\bullet+}$) is seen in many types of PAH spectra and is produced here by three different dissociation pathways (Figure 1) from $C_{16}H_{10}^{\bullet+}$. The remarkable similarity between the fragment ions produced and the neutral losses observed for different PAH compounds under various activation methods has been interpreted as a result of rapid isomerization to yield common intermediate structures. Furthermore, it has been suggested that the polycyclic PAH structure might linearize in a stepwise process, isomerizations occurring in concert with progression through the dissociation sequence.[7] A number of studies on large (C_{10} to C_{29}) all-carbon molecules suggest that the carbons are connected to form monocyclic rings with alternating C—C and C≡C bonds.[54,55]

In order to provide further information on PAH fragmentations, CAD of anthracene was studied (Figure 4). Common losses of H•, C_2H_2, and C_4H_2 are analogous to those seen in the fragmentation of pyrene. The longest sequence of dissociations is represented by nine separate isolation and activation steps from one ionization event (MS^{10}). The common ion at m/z 150 ($C_{12}H_6^{\bullet+}$) is again an important intermediate, with a fragmentation pattern similar to that observed in the pyrene system. Thus, this ion may well have the same structure (or mixture of structures) in both instances.

Ions resulting from CH_n losses from $C_{16}H_{10}^{\bullet+}$ are seen in low abundances in all high-energy MS/MS experiments performed here. It has been suggested that CH_n loss may be particularly sensitive to the type of activation method used as well as the shape of the internal energy distribution curve,[7] and the present results support this. This process is observed in high- and low-energy CAD experiments, but it occurs only to a very small extent in MPI, PD, and SIMS where fragmentation takes place in the ion source (ion residence times are less than a microsecond). It is favored in FTMS where residence times can exceed several hundred milliseconds.[7] Although this is a fairly high energy pathway (approximately 12 eV for phenanthrene[23]), it is not generally observed in EI experiments, probably because the single ionization and activation step in this experiment does not facilitate the rearrangements necessary for this entropically demanding process.[7,23,56] The ion-trap mass spectrometer has the unique ability to allow highly energetic collisions, which result in the formation of fragment ions such as m/z 98 ($C_8H_2^+$) and, in addition, extremely long residence times, which concurrently result in the presence of rearrangement ions which would otherwise be kinetically unfavorable.

The structures of doubly-charged PAH ions, generated by EI and by high-energy CAD, have also been of interest.[56-58] The fragmentation patterns obtained for singly-charged ions formed by dissociative charge-exchange of doubly-charged molecular ions are similar to those of singly-charged ions generated by EI,[7] suggesting that the structures for the stable singly-charged and doubly-charged ions are similar, viz., that the latter are polycyclic. Fragmentation data, such as that shown in Scheme II, support this analogy as do other mass spectrometric methods used to study doubly-charged pyrene ($C_{16}H_{10}^{2+}$).[7,56-58] The occurrence of both charge-separation fragment ions and fragment dications is a characteristic feature of PAHs, but the issue of whether the charge-separation processes are associated with ring opening is not resolved.[59]

While the CAD efficiency for single MS/MS steps in an ITMS is often high (nearly 100%),[39] the efficiency for MS^n experiments is much lower.[43,45] This is an inevitable consequence of the fact that a single ion is selected from among the CAD products to serve

(54) Rubin, Y.; Knobler, C. B.; Diederich, F. *J. Am. Chem. Soc.* **1990**, *112*, 1607.
(55) Diederich, F.; Rubin, Y.; Knobler, C. S.; Whetten, R. L.; Schriver, K. E.; Houk, K. N.; Li, Y. *Science* **1989**, *245*, 1088.
(56) Ast, T.; Beynon, J. H.; Cooks, R. G. *Org. Mass Spectrom.* **1972**, *6*, 749.
(57) Mathur, B. P.; Burgess, E. M.; Bostwick, D. E.; Moran, T. F. *Org. Mass Spectrom.* **1981**, *16*, 92.
(58) Cooks, R. G.; Ast, T.; Beynon, J. H. *Int. J. Mass Spectrom. Ion Phys.* **1973**, *11*, 490.
(59) Koyanagi, G. K.; March, R. E. *Int. J. Mass Spectrom. Ion Processes* **1988**, *83*, 245.

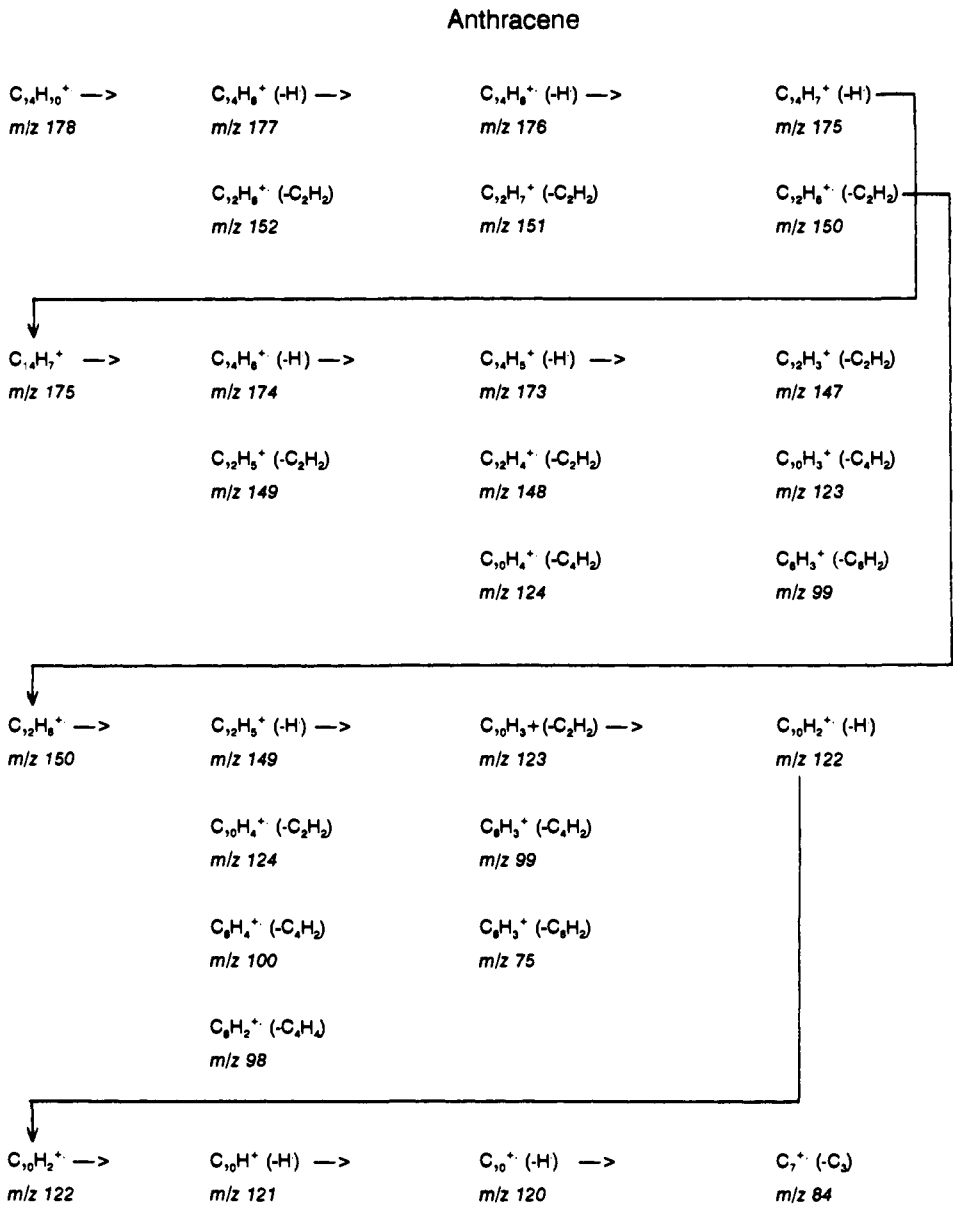

Figure 4. Consecutive dissociation pathways of ionized anthracene determined by using CAD in an ITMS. An ac amplitude of 1 V_{p-p} was applied to each isolated ion for 50 ms.

as the precursor for subsequent CAD steps. On the other hand, in the single-stage high-activation-energy CAD experiments, simulations of ion motion[60] show that ejection of ions occurs during activation, and this contributes to the loss of ion signal. The CAD efficiencies for anthracene are higher than for pyrene (Table IV), and this is attributed to the lower activation energies required to dissociate the smaller ion. Previous studies have shown that the CAD efficiency is higher under lower excitation conditions.[39] The overall yield of the MS^{10} product ion, $C_7^{\cdot+}$ (m/z 84), compared to the anthracene molecular radical cation (m/z 178), is 0.34%.

In order to estimate the maximum amount of internal energy which can be transferred to an ion population in the course of activation in the ion trap, the dissociation sequence shown in Scheme I was carried out. The critical energies for each reaction, the minimum energy required to form product ions, are estimated from heats of formation for the ions and neutrals ($\Delta(\Delta H_f) = \Delta H_{rxn} \simeq \epsilon_0$) as shown in the supplementary material. The uncertainties determined for each ϵ_0 value reflect uncertainties in the ΔH_f values. Heats of formation for many of the intermediate ions are not available, and in these cases, estimates were made by comparisons with similar reactions[9] or by extrapolation from known values.

(60) Julian, R. K., Jr.; Reiser, H. P.; Cooks, R. G. To be published.

In either case, the accuracy of the estimated activation energies is dependent on that of the reference values. Errors can arise from many sources, including kinetic shifts and nonnegligible reverse activation energies, and these factors may carry forward some internal energy from one stage of the experiment to the next. In addition, the structures of the intermediate ions are not always certain and, when necessary, structures are assumed. The uncertainties represented in Scheme I do not include errors due to inaccuracies in structural assignment of the intermediate ions or the carry-forward of internal energy.

Although each individual dissociation step requires ≤8 eV, the overall energy required to convert m/z 202 to m/z 62 is roughly given by the sum of the critical energies, which is approximately 29 eV. The success of this multiple activation experiment demonstrates that it is possible to deposit large amounts of energy (tens of electronvolts) into ionized pyrene using the ITMS, even though it is emphasized that this energy is not deposited in a single stage of activation and that the value is only a rough estimate for the reasons just given. The maximum energy deposited in one stage of activation under normal conditions does not exceed 8 eV, a value consistent with earlier estimates based on other polyatomic ions which show maximum energy depositions of up to 6.0 eV.[39,46] Note again that even during a single stage of activation many collisions

occur; the 50-ms activation time corresponds to 5×10^4 rf cycles, and simulations suggest[60] that up to 10^4 collisions with helium can occur in this time. The possibility that large internal energies might be deposited in a single collision with helium can be readily excluded on kinematic grounds. The average kinetic energy for the pyrene molecular ion (under these experimental conditions) is 28 eV, based on Dehmelt's pseudo-potential-well model.[61] Therefore, an average internal energy imparted into the parent ion as the result of a single collision with a helium target is approximately 0.5 eV, which is insufficient to cause extensive fragmentation. The deposition of large amounts of energy may occur incrementally in a series of collisions prior to fragmentation of the parent ion. However, the internal energies deposited are expected to cause dissociation at rates which are fast relative to the time between collisions, which is estimated to be quite long (ca. 10^{-7} s).[60] This competition between fragmentation and further activation should result in overwhelming formation of lower energy product ions. The resonance frequency of these ions (reactant and product) is dependent on mass, and therefore the product ions require a distinct frequency for resonance excitation and are not expected to be efficiently activated as a result of further collisions with the helium buffer. However, under extreme activation conditions (12 V_{p-p}), a wide mass range of off-resonance ions can be activated.[63] Subsequent dissociation of lower energy fragments does produce high-energy fragments in a single MS/MS step. Collisions with surfaces might also play a role in the fragmentation process. Simulations[60] suggest that such collisions with the endcap electrodes do indeed occur under the extreme conditions employed in these particular activation experiments.

A second type of activation experiment was carried out to address the question of whether still higher energies could be deposited during a single stage of activation. The CAD spectrum for the pyrene molecular radical cation was recorded under extreme activation conditions, principally by increasing the amplitude of the ac voltage used to effect activation (Figure 3). This experiment resulted in the formation of an ion at m/z 122 ($C_{10}H_2^{\bullet+}$), a process not observed under normal CAD conditions and which requires between 17 and 22 eV, depending on the dissociation pathway taken (see supplementary material). As a consequence of the high-excitation conditions used, the overall CAD efficiency is significantly lower than that measured using normal activation conditions. This result demonstrates that one can deposit large amounts of internal energy into ions in a single-stage MS/MS experiment, albeit at the expense of CAD efficiency and by a mechanism which is not completely elucidated. However, since off-resonance excitation of lower energy fragment ions can occur during this MS/MS stage,[63] the formation of high-energy fragments may still be occurring in a stepwise fashion.

In a third type of activation experiment, a small proportion of xenon was introduced with the helium buffer gas, and a greater relative abundance of the higher energy fragments was observed. This is in agreement with earlier studies which examined the effects of heavier target gases on dissociation processes.[47-50] The heavier target gas is expected to result in higher center-of-mass collision energies; a single collision with a xenon target is estimated from the kinetic energy estimated by the Dehmelt model[61] to deposit a maximum internal energy of 22 eV into the parent ion. Internal energies necessary to dissociate the molecular ion to yield high-energy product ions are therefore readily available. Table II compares the results of MS/MS experiments using helium alone with those using the helium/xenon mixture. The overall CAD efficiencies of the two processes are roughly comparable, but the experiments involving mixed target gases result in more abundant, higher energy fragments. The experiments represented in Table II were performed using resonance ejection for enhanced sensitivity, resulting in much higher CAD efficiencies.

The high CAD efficiency achieved in conjunction with high internal energy deposition in the mixed-gas experiment (Table III) is due, in part, to the method used for parent ion isolation. The traditional means of isolation involves applying a combination of rf and dc voltages to bring the parent ion to the cusp of the Mathieu stability diagram, where collisions with a heavy target gas during the isolation process can result in scattering of the ion and ejection from the trap. When isolation is performed using the rf-only method, the parent ion remains on the $a_z = 0$ line, and collisions with xenon have a smaller probability of leading to ion loss due to scattering. In this experiment, the ion trap may be viewed as being operated in a mode similar to that used when an rf-only quadrupole is used as a collision region in a triple quadrupole mass spectrometer.[62] The rf-only quadrupole has a high efficiency of ion transmission to the mass-analyzing quadrupole following the collision process. Tables II and III compare the two methods of isolation (rf/dc and rf alone) and show higher CAD efficiencies and more extensive fragmentation when the rf-only mode of isolation is utilized.

Conclusion

This study has employed multiple isolation and dissociation steps to characterize the fragment ions generated from selected singly- and doubly-charged PAH molecular ions. The types of fragmentations observed in the ion trap correspond well with those recorded by other activation methods. Long reaction sequences have been characterized (e.g., by MS^{10} experiments), and they show familiar PAH ion chemistry. Also, utilizing the MS^n capability of the ITMS, high-energy CAD pathways are accessed (tens of electronvolts) through a series of sequential low-energy dissociations. Direct access to high-energy pathways such as $C_{16}H_{10}^{\bullet+} \rightarrow C_{10}H_2^{\bullet+}$ (estimated 17-eV activation energy) is possible under extreme activation conditions, although at a cost in terms of efficiency. However, using a mixture of target gases and using rf-only parent ion isolation, one can achieve high internal energy deposition with high CAD efficiency.

Acknowledgment. This work was supported by the National Science Foundation (CHE87-21768). We thank R. R. Squires for valuable discussions.

Registry No. Pyrene, 129-00-0; anthracene, 120-12-7.

Supplementary Material Available: Estimated activation energies for the dissociation reactions of Scheme I, the total activation energy for the overall reaction $C_{16}H_{10}^{+} \rightarrow C_{10}H_2^{+}$, and a table listing heats of formation used to estimate activation energies for the sequential dissociation of pyrene (11 pages). Ordering information is given on any current masthead page.

(61) Major, F. G.; Dehmelt, H. G. *Phys. Rev.* **1968**, *179*, 91.

(62) Yost, R. A.; Enke, C. G. *J. Am. Chem. Soc.* **1978**, *100*, 2274.

(63) Nourse, B. D.; Wise, M. B.; Buchanan, M. V. Unpublished results.